Polish Polar Research
DOI: 10.24425/ppr.2026.3128

Covariation of dissolved nutrients and carbon in seawaters and sediment porewaters of western Svalbard fjords

Seyed Reza SAGHRAVANI[1]* ORCID-0000-0002-0140-7887, Arunima SEN[2] ORCID-0000-0001-7847-2137, Wei-Li HONG [3,4] ORCID- 0000-0002-7247-1827 and Marc J. SILBERBERGER[5] ORCID-0000-0001-8819-4388

[1] *Institute of Oceanology Polish Academy of Sciences, Powstańców Warszawy 55, 81-712 Sopot, Poland*
[2] *Department of Arctic Biology, University Centre in Svalbard, N-9171, Longyearbyen, Norway*
[3] *Department of Geological Sciences, Stockholm University, Svante Arrhenius väg 8, 11418 Stockholm, Sweden*
[4] *Baltic Sea Centre, Stockholm University, Universitetsvägen 10 A, 10691 Stockholm, Sweden*
[5] *Department of Fisheries Oceanography and Marine Ecology, National Marine Fisheries Research Institute, Hugo Kołłątaja 1, 81-332 Gdynia, Poland*

***corresponding author:** reza@iopan.pl

Received 8 May 2026 **Accepted** 22 July 2026

Running title: Carbon–nutrient variability in Svalbard fjords

Abstract: We analyzed dissolved inorganic and organic carbon as well as dissolved inorganic nutrient concentrations in surface waters, bottom waters, water above sediments (*i.e.,* core-top water), and sediment porewaters at 19 sites in western Svalbard fjords. Multiple Factor Analysis was used to identify common patterns in the water column and sediment layers. The analysis revealed a clear separation between surface waters and all deep water and porewater layers due to the strong summer stratification. Bottom waters, water above sediments, and both upper and lower porewater layers showed strong covariation across sites, with some sites consistently exhibiting low concentrations of carbon and nutrients, and others high concentrations across these layers. In contrast, surface

water concentrations varied more independently from the other layers. Most of the variation among deep water and porewater layers was driven by a small number of sites that showed enrichment in dissolved inorganic carbon, dissolved organic carbon, and multiple nutrients in bottom waters and porewaters. Differences among sites in fjords often exceeded those between fjord systems, suggesting that deep water and porewater biogeochemical variability is structured more strongly by local basin conditions than by fjord-wide gradients. The strong covariation between bottom water and porewater chemistry suggests that bottom water concentrations integrate sedimentary signals at sites. This fine-scale, basin-level heterogeneity implies that fjord-averaged descriptions overlook biogeochemically distinct basins and that resolving individual basins and secondary fjords is necessary to anticipate how these systems respond to ongoing Arctic change. The patterns are likely shaped by local hydrographic conditions, including winter water formation, Atlantic Water intrusion, and freshwater inputs, all of which are changing rapidly in Arctic fjords. These changes may alter the persistence of local enrichment patterns and complicate predictions of future nutrient and carbon dynamics.

Keywords: Arctic, Spitsbergen, porewater, surface water, bottom water.

Introduction

Arctic fjords are semi-enclosed transition zones where terrestrial and marine materials are transformed, retained, and redistributed under the combined influence of glacial, oceanic, and sedimentary processes (Syvitski 1989; Azetsu-Scott and Syvitski 1999). In Svalbard, fjords are density-stratified in summer, and deep water properties vary among fjords depending on sill depth and circulation. Some fjords contain Atlantic-influenced water at depth, whereas others, particularly silled inner basins, retain cold, locally formed winter-cooled water year-round (Cottier *et al.* 2005; Nilsen *et al.* 2016; Skogseth *et al.* 2020). This density stratification limits vertical exchange and influences the distribution of nutrients and carbon between surface waters dominated by photosynthetic processes and deeper waters where remineralization predominates (Sejr *et al.* 2017).

While vertical gradients in dissolved inorganic and organic carbon and nutrient concentrations in the water column are reported in some Arctic fjords (Ericson *et al.* 2019b; McGovern *et al.* 2020), recent work has quantified seawater and porewater gradients in western

Spitsbergen fjords (Saghravani *et al.* 2024). Less is known, however, about how these layers vary spatially across sites. Sediment porewaters often have elevated nutrient and carbon concentrations that far exceed those in overlying waters, creating steep gradients at the sediment–water interface and promoting benthic–pelagic exchange (Huettel *et al.* 2014). However, it remains unclear whether nutrient and carbon concentration variability in surface waters, deep waters, and sediment porewaters responds to environmental controls, or whether distinct processes dominate different layers.

Freshwater inputs to Arctic fjords, including glacial meltwater, river discharge, and submarine groundwater discharge, deliver chemically distinct waters and organic matter to coastal environments, contributing pronounced spatial heterogeneity in nutrient and carbon concentrations (McGovern *et al.* 2020; Santos *et al.* 2021). In the Arctic, the influence of freshwater pathways is increasing as permafrost thaw and glacial retreat alter subsurface hydrology and create new routes for nutrient and carbon transport (Diak *et al.* 2023; Kleber *et al.* 2023). Where freshwater inputs interact with restricted circulation and limited deep water renewal, nutrients and both inorganic and organic carbon may accumulate in bottom waters. By contrast, nearby locations with stronger water exchange may remain comparatively low. As a result, sites of elevated nutrient and carbon concentrations may occur immediately adjacent to less enriched areas within the same fjord, suggesting that biogeochemical variability is structured by local hotspots associated with freshwater inputs, restricted deep-water renewal, and sediment organic matter supply rather than by fjord-scale gradients.

In this study, we assess whether dissolved inorganic and organic carbon, as well as nutrient concentrations, covary between surface waters, deep waters, and sediment porewaters in western Svalbard fjords or whether concentrations are controlled by layer-specific processes. We analyze concentrations of inorganic nutrients, inorganic and organic carbon in surface waters, deep waters, and sediment porewaters at multiple sites in western Svalbard fjords. To identify patterns among layers while accounting for differences in concentration magnitude, we apply multiple factor analysis (MFA) (Abdi *et al.* 2013), to the combined water column and porewater dataset. MFA is a multivariate ordination method that extends principal component analysis to datasets organized into predefined groups of variables measured on the same observations. MFA, which has recently been applied to characterize geochemical variability in Arctic marine porewater systems (Saghravani 2026), allows us to evaluate benthic–pelagic coupling and to

determine whether spatial variability is primarily organized at the scale of individual sites or reflects broader fjord-scale gradients.

Study area

Svalbard is a High Arctic archipelago located between 74° and 81°N. The West Spitsbergen Current transports warm and saline Atlantic Water northward along the western coast, penetrating fjord systems to varying degrees depending on fjord morphology and sill depth (Cottier *et al.* 2005). Three fjord systems along western Spitsbergen, the largest island in the archipelago, were selected for this study: Hornsund in the south, Isfjorden in central Spitsbergen, and the connected Kongsfjorden-Krossfjorden system in the north (Fig. 1).

Hornsund is a relatively small fjord (~30 km long, 2–5 km wide) with more than ten marine-terminating glaciers that deliver large sediment loads via glacial discharge to the fjord (Smith *et al.* 2015; Pawłowska *et al.* 2016). The fjord consists of an outer basin (~180 m deep) and an inner basin (Brepollen) separated by a sill at approximately 50 m water depth. This sill limits exchange between the basins, and bottom waters are typically cold throughout the fjord (−1.2 to 1.6°C) (Promińska *et al.* 2018). Bedrock in the Hornsund catchment is dominated by Precambrian granitic and metamorphic rocks (Görlich 1986).

Isfjorden is the largest fjord system in Svalbard and includes several secondary fjords with contrasting hydrographic settings. Inner secondary fjords such as Billefjorden and Tempelfjorden are characterized by shallow sills that restrict deep-water exchange, whereas outer secondary fjords (*e.g.,* Adventfjorden) are more open to the influence of shelf waters (Szczuciński *et al.* 2009). Although Atlantic Water influences Isfjorden overall, its penetration varies among fjord basins: inner silled fjords such as Billefjorden retain cold winter water, whereas outer areas experience warmer conditions due to greater Atlantic Water intrusion (Saghravani *et al.* 2024). The Isfjorden catchment is underlain by complex Paleozoic and Mesozoic sedimentary sequences, including hydrocarbon-bearing strata (Roy *et al.* 2015) that influence organic carbon cycling in the fjord's sediments (Szymczycha *et al.* 2025).

Kongsfjorden and Krossfjorden are connected fjords in northwestern Spitsbergen with open connections to the continental shelf, allowing frequent intrusions of Atlantic Water, similar to the outer parts of Isfjorden (Hop *et al.* 2002; Piwosz *et al.* 2009). As a result, bottom waters are generally warmer (1.9–2.9°C) than in Hornsund and the inner, silled secondary fjords of

Isfjorden (such as Billefjorden). Kongsfjorden and Krossfjorden receive freshwater and sediment inputs from marine-terminating and land-terminating glaciers. The surrounding bedrock consists of mixed sedimentary and metamorphic sequences, including marble and carbonate-bearing units (Svendsen *et al.* 2002).

Methods

Sampling design and water layers

Sampling was conducted aboard the R/V *Oceania* between July and September in 2021 and 2022 as part of the Arctic Expedition (AREX), the long-term multidisciplinary Arctic monitoring program of the Institute of Oceanology, Polish Academy of Sciences. A total of 19 sites were sampled in the three western Svalbard fjord systems, as illustrated in Fig. 1. Water column depths at the sampling sites ranged from 33 to 374 m (Table 1).

At each site, a single sample was collected from each of five layers: (*i*) surface water (0-2 m depth), (*ii*) bottom water (2–3 m above the seafloor), (*iii*) water directly overlying the sediment (*i.e.* water contained within the sediment core liner above the sediment-water interface; water above sediment), (*iv*) upper sediment porewater (1–7 cm sediment depth), and (*v*) lower porewater (21.5–280 cm sediment depth, representing the deepest porewater interval recovered at each site, depending on core penetration). The upper porewater interval represents near-surface sediments influenced by benthic exchange, bioturbation, and bioirrigation, whereas the deeper porewater interval reflects more isolated geochemical conditions below the main zone of macrofaunal influence.

Surface and bottom waters were collected using a Sea-Bird Scientific SBE 911 Plus conductivity–temperature–depth (CTD) rosette profiler equipped with 10-L Niskin bottles and an SBE 43 oxygen module (calibrated prior to the cruise). Sediment cores were collected with a gravity corer. Sediment porewaters were extracted through pre-drilled holes in the core liners using Rhizon® samplers (Rhizosphere, 2.5 mm diameter, mean pore size 0.15 µm). In addition, either a GEMAX or a Niemistö corer were deployed at the same locations to collect water directly overlying the sediment (Saghravani *et al.* 2024). Water overlying the sediment surface in the core liner was collected immediately after core retrieval using a syringe carefully inserted into the overlying water column within the core liner, avoiding disturbance of the sediment-water interface.

Sample handling and preservation

Upon collection, each water sample was sub-sampled into several aliquots for different analyses. For inorganic nutrient analyses (ammonium – NH_4^+, nitrate – NO_3^-, phosphate – PO_4^{3-}, dissolved silica – DSi), up to 5 mL of porewater was transferred into pre-cleaned (rinsed with Milli-Q water) high-density polyethylene (HDPE) bottles, and 10 mL of seawater was filtered through 0.45 µm cellulose acetate filters into pre-cleaned (rinsed with Milli-Q water) HDPE bottles. All sub-samples were then stored frozen at −20°C until analysis. Sub-samples for dissolved inorganic carbon (DIC) were collected in gas-tight glass bottles (250 mL for seawater, 12 mL for porewater), poisoned with a saturated $HgCl_2$ solution (25 µL for porewater, 100 µL for seawater), and stored without headspace to prevent biological activity and gas exchange. For dissolved organic carbon (DOC) analysis, 20 mL and 12 mL of seawater and porewater, respectively, were filtered through 0.45 µm MN GF-5, acidified with HCl to pH ~2, and stored at 4°C until analysis. Approximately 2 mL of sample for chloride (Cl^-) analysis was transferred to PET vials, which were stored at 4°C. Approximately 10 mL of porewater samples for major cation analysis were acidified with ultrapure HNO_3 to a pH < 2 and stored at 4°C until measurement.

Laboratory analysis

Nutrient concentrations were determined using a SEAL AA500 AutoAnalyzer (Seal Analytical) with standard photometric methods (Grasshoff *et al.* 1999). Quality control included repeated measurements of two Certified Reference Materials (QC3179 from Sigma Aldrich, and HAMIL from Environment Canada). The accuracy of NO_3^-, NH_4^+, PO_4^{3-}, and DSi measurements was 98.8%, 98.8%, 99.0%, and 100.1%, respectively. The precision was 0.01 µmol L^{-1}, 0.02 µmol L^{-1}, 0.01 µmol L^{-1}, and 0.03 µmol L^{-1}, respectively (the reported NO_3^- values are nitrate only and do not include nitrite). Cl^- concentrations were determined by potentiometric titration to a precision of 0.1 mmol L^{-1} (Kłostowska *et al.* 2020). DIC analyses were conducted with Apollo SciTech's AS-C6L DIC Analyzer, which features a laser-based CO_2 detector (LI-7815, Li-Cor, USA). Measurement accuracy was ensured by analyzing certified reference materials (CRMs, batches #190 and #195) from A.G. Dickson (Scripps Institution of Oceanography, USA). Precision was assessed from triplicate measurements of individual samples and was no worse than ±3 µmol L^{-1}, with an average recovery of 99.0%. DOC analyses were conducted on a TOC-

L analyzer (Shimadzu) using a high-temperature (680°C) oxidation method with a Pt catalyst. The precision of DOC measurements was ±4 µmol L^{-1}. Accuracy was determined by repeated measurements of certified reference materials (CRMs) provided by the D. Hansell Laboratory (University of Miami, USA), with a recovery of 99%. Major cations were measured using a flame atomic absorption spectrometer (AAS; Shimadzu AA-6800 Series). Samples were diluted 10-to 100-fold with ultrapure water before AAS analysis to bring concentrations within the instrument's optimal range. Analytical precision was < 2% relative standard deviation for all cations, with detection limits of 0.4 µmol L^{-1} (0.01 mg L^{-1}) for sodium (Na^+), 0.26 µmol L^{-1} (0.01 mg L^{-1}) for potassium (K^+), 0.12 µmol L^{-1} (0.005 mg L^{-1}) for calcium (Ca^{2+}), and 0.21 µmol L^{-1} (0.005 mg L^{-1}) for magnesium (Mg^{2+}). Accuracy was verified using a certified reference material (CASS-6 seawater standard), yielding recoveries of 95-105% for all elements. Cation concentrations were converted to mmol L^{-1} for all subsequent analyses.

Data organization and multiple factor analysis

MFA was used to investigate spatial covariation among nutrient and carbon concentrations measured in the water column and sediments. In simple terms, MFA was used to assess whether dissolved nutrient and inorganic and organic carbon concentrations showed similar spatial patterns in the water column and sediment layers among sampling sites.

Variables were grouped by sampling layer. Accordingly, five groups of active variables were defined: surface water, bottom water, water above sediment, upper sediment porewater, and lower sediment porewater. Each group contained the same six chemical variables: DIC, DOC, NH_4^+, NO_3^-, PO_4^{3-}, and DSi. This resulted in a dataset comprising 30 active chemical variables (6 variables × 5 distinct layers) across 19 sampling sites.

Environmental variables describing hydrographic and site characteristics were included as supplementary variables to aid interpretation of ordination patterns. These included water depth, sediment core length, bottom water temperature, distance from land, distance from glaciers, distance from rivers, Cl^- concentrations in surface water and lower porewater, and major cation concentrations (Na^+, K^+, Ca^{2+}, Mg^{2+}) measured in water overlying the sediment and in porewaters. Supplementary variables were projected onto the MFA ordination space after analysis and therefore did not influence the calculation of the MFA dimensions.

Prior to analysis, all active variables were standardized to unit variance to account for differences in concentration ranges across the five sampled layers. Following standard MFA

procedures, each layer, treated as a separate group of variables, was weighted by its internal variance structure to ensure equal contribution to the overall analysis. Although each layer contained the same set of chemical variables, this weighting accounts for differences in the correlation structure within each layer, preventing any single layer from exerting a disproportionate influence on the results. Consequently, the analysis extracts a set of new axes, referred to as dimensions, that represent the main patterns of variation shared across the water column and porewater layers. Each dimension summarizes a set of chemical variables that vary together in samples. The position of a layer relative to a dimension, referred to as its group loading, indicates how strongly that layer reflects the shared pattern, whereas the position of an individual variable indicates the direction and strength of its association with that pattern with values near 1 indicating close alignment and values near 0 indicating little association.

Results

Vertical distribution of chemical concentrations

Clear vertical gradients were observed for most dissolved carbon and nutrient species in the five layers (Fig. 2). DIC, DOC, NH_4^+, PO_4^{3-}, and DSi showed low concentrations in surface and bottom waters, modest increases in water above sediment, and higher concentrations in sediment porewaters. For example, DIC rose from ~1900–2110 µmol L^{-1} in surface waters to 2650–21260 µmol L^{-1} in lower porewaters; NH_4^+ from < 0.3–2.4 to 87–773 µmol L^{-1}; DOC from 19–85 to 230–2690 µmol L^{-1}; PO_4^{3-} from 0.1–0.4 to up to ~75 µmol L^{-1}; and DSi from 0.7–2.8 to up to ~290 µmol L^{-1}. In particular, DIC and NH_4^+ concentrations increased sharply from the water column to the porewaters. NO_3^- showed a different pattern: concentrations were low in surface waters (0.3–3.7 µmol L^{-1}), higher in bottom waters and water above sediment (up to ~13–14 µmol L^{-1}), and declined in both upper and lower porewaters.

Cl^- and major cations measured in water above sediment and in porewaters showed variable distributions without a consistent monotonic vertical pattern. As expected in these marine systems, Na^+ tracked Cl^- conservatively; Ca^{2+}, K^+, and Mg^{2+}, in contrast, showed site-specific variability, particularly in the lower porewaters.

Across-fjord variability

Nutrient and dissolved (in)organic carbon concentrations in surface water, bottom water, water above sediment, and porewaters were broadly similar across the fjord systems (Fig. 3). For most

variables, interquartile ranges and medians overlapped among the three fjord systems. NO_3^-, NH_4^+, DSi, and PO_4^{3-} concentrations varied considerably among fjords, particularly in Isfjorden, but no differences among fjord systems were evident. DOC concentrations showed greater variability in Hornsund and Isfjorden than in Kongsfjorden and Krossfjorden, although the concentration ranges overlapped. Similarly, DIC and Cl^- concentrations showed no clear separation among fjords. Major cation concentrations (Na^+, Ca^{2+}, K^+, Mg^{2+}) varied across sites but did not differ by fjord. Overall, variability among sites within fjords was comparable to, or even greater than, that between fjord systems.

Multiple factor analysis

The first three MFA dimensions (composite axes representing the main patterns of chemical variation across sites) accounted for 57.4% of the total variance (29.9%, 14.4%, and 13.2% for dimensions 1 to 3, respectively). Together, the first five dimensions explained 73.5% of the total variance (Table 2).

Dimension 1 was strongly represented by bottom water, water above sediment, and upper and lower porewater layers (group loadings 0.65-0.72, *i.e.*, these layers align closely with this axis), whereas surface water showed a weak association with this dimension. Site contributions to Dimension 1 were uneven, with SGD9 accounting for 40.8% of the variance, followed by SGD4 (18.0%) and SGD3 (14.6%). Dimension 2 is represented mainly by surface water (loading 0.56) and upper porewater (loading 0.40). Sites SGD27 and SGD5 contributed 23.9% and 11.0%, respectively, to the variance explained by this dimension. Dimension 3 was represented primarily by surface water (loading 0.50), whereas bottom water showed a weaker association (0.32). SGD5 contributed 39.2% to the variance in Dimension 3, followed by SGD25 (13.0%). Taken together, the first three dimensions indicate that surface water chemistry varied largely independently of the deep water and porewater layers.

At the variable level, Dimension 1 was characterized by high positive coordinates (0.70–0.90) for DOC, DSi, and PO_4^{3-} in the bottom water and porewater groups, indicating that these variables increase together across sites. By contrast, surface water variables had near-zero coordinates on Dimension 1, indicating that they were largely unrelated to deep water and porewater patterns. Dimension 2 was associated with surface water NO_3^-, PO_4^{3-}, and NH_4^+, along with selected porewater variables. Dimension 3 was driven mainly by surface water DIC, NO_3^-, and PO_4^{3-} concentrations. The MFA biplots visualize relationships among variables, layers, and

sites along the main dimensions of variation (Fig. 4). In the Dimension 1–Dimension 2 projection, bottom water, water above sediment, and porewater variables cluster along the positive side of Dimension 1, indicating that they increase together across sites, whereas surface water variables align along Dimension 2, reflecting a distinct pattern of variation. In the Dimension 1–Dimension 3 projection, surface-water variables are separated primarily along Dimension 3. Sites contributing most strongly to Dimension 1, particularly SGD9, are located at the positive end of this axis.

Discussion

Deep water and porewater coupling and surface water decoupling

Across most sites in all three fjord systems, concentrations of carbon and nutrients in bottom water, water above sediment, and both porewater layers showed coordinated variation, whereas concentrations in surface waters varied independently. This coupling is the dominant pattern captured by the MFA: the four deep water and porewater layers load strongly on Dimension 1 (0.65–0.72), meaning their variables align closely with this axis, whereas surface water does not. Dimension 1 separates sites with relatively low versus high concentrations of nutrients and carbon in deep waters and porewaters, explaining 29.9% of the total variance (Fig. 4). Variables including NO_3^-, PO_4^{3-}, DSi, DOC, and DIC from several layers are similarly distributed along this dimension, indicating that enrichment occurs simultaneously across multiple constituents rather than in isolated variables.

The similarity between bottom water and water above sediment on Dimension 1 indicates strong covariation between near-bottom water and sediment porewater chemistry. Sites with high porewater concentrations of nutrients and carbon showed elevated bottom water concentrations, supporting the interpretation that bottom water chemistry reflects integrated sedimentary biogeochemical conditions at the site scale (Kostka *et al.* 1999). This interpretation is supported by the concentration profiles (Fig. 2), which show coordinated increases in carbon and nutrient concentrations from bottom water through water above sediment into the porewaters. It is further supported by their relationships with Cl^- (Fig. 5), where porewater DIC, DOC, NH_4^+, PO_4^{3-}, and DSi concentrations lie well above the conservative seawater–freshwater mixing line, indicating that the enrichment reflects in-situ remineralization rather than physical mixing. Importantly, the sites contributing most strongly to this pattern are characterized by concurrent enrichment in DIC,

DOC, NH_4^+, PO_4^{3-}, and DSi rather than by elevated concentrations of any single variable. This coordinated enrichment across multiple carbon and nutrient species indicates that organic-matter remineralization in the sediments is the common driver of these chemical patterns, with its products accumulating in the porewaters and the overlying bottom water.

Sites with deeper water columns often showed elevated concentrations in bottom water, water above sediment, and porewaters. The weak relationship ($r = 0.42$) reflects variation in basin ventilation: deep basins behind shallow sills often accumulate remineralization products due to limited exchange and long residence times, whereas similarly deep but more open basins are better ventilated (Skogseth *et al.* 2005; Inall and Gillibrand 2010).

Conversely, surface water had little impact on Dimension 1 but was the primary driver of Dimensions 2 and 3. The orientation of surface nutrient variables along these secondary dimensions indicates that surface water variability is organized separately from the main deep water and porewater pattern. This separation aligns with the strong summer stratification observed in Arctic fjords, which restricts vertical mixing and allows surface processes, such as biological uptake, atmospheric exchange, and freshwater input, to proceed independently of deep water and sediment activities (Cottier *et al.* 2005; Stigebrandt 2012; McGovern *et al.* 2020; Meyer *et al.* 2020).

Biogeochemical hotspots and basin morphology

A small number of sites account for a disproportionate share of the coordinated deep water and porewater enrichment. Three sites (SGD9 in Billefjorden, Isfjorden; SGD3 and SGD4 in the main basin of Hornsund), representing 16% of sampled sites, explained 73.4% of the variance in Dimension 1. These sites are located in basins with limited deep-water exchange, where water depth exceeds the sill depth, promoting prolonged isolation of dense bottom waters (Inall and Gillibrand 2010). The site in silled Billefjorden recorded the coldest bottom water temperature during the study period (−1.7°C), consistent with locally formed winter water and limited renewal (Cottier *et al.* 2005). SGD3 and SGD4 lie in the main basin of Hornsund, where water depth (181 and 240 m) exceeds the ~150 m depth at the fjord entrance, favoring isolation of dense bottom water. In this case, bottom water is warmer than in Billefjorden (> 1°C) but is overlain and isolated by Atlantic Water (Swerpel 1985). In contrast, sites in well-ventilated settings, including SGD32 at the mouth of Kongsfjorden, showed little deep water and porewater enrichment despite

reaching depths of 374 m. Frequent Atlantic Water intrusions at this location probably hinder the continual accumulation of remineralization products (Tverberg *et al.* 2019).

Basin isolation alone, however, does not fully explain enrichment patterns. For example, SGD1 in Brepollen, the inner deep basin of Hornsund, lies behind a shallow sill, has cold bottom water, yet shows slight enrichment in deep water and porewater. One possible explanation is that increased exchange is linked to submarine groundwater discharge, indicated by Cl^- depletion in lower porewaters (Table 1) and by previous reports of hydrological connectivity in Arctic fjords (Taniguchi *et al.* 2019; McGovern *et al.* 2020). Although the co-occurrence of Cl^- depletion and nutrient/carbon enrichment at SGD3 and SGD4 is consistent with a groundwater contribution, submarine groundwater discharge is characteristically low in DIC and nutrients and cannot, by itself, account for the magnitude of enrichment observed; in-situ remineralization is therefore required, with groundwater discharge potentially modulating the physical environment. Alternatively, the inner part of Hornsund may experience a reduced influence from Atlantic Water relative to SGD3 and SGD4, potentially limiting the supply of labile marine organic matter to sediments and thereby constraining remineralization rates despite physical isolation. Although these mechanisms cannot be determined from the present dataset, contrasting behavior among morphologically similar basins suggests that basin restriction and organic matter supply influence hotspot formation.

Secondary dimensions revealed distinct surface-dominated patterns. SGD5 in inner Hornsund accounted for 39.2% of the variance in Dimension 3 due to elevated surface DIC and nutrient concentrations, whereas SGD27 in Nordfjorden (Isfjorden) drove Dimension 2. These two sites stood out for surface-layer enrichment rather than subsurface coupling: SGD5 in inner Hornsund, with markedly elevated surface DIC and nutrient concentrations, and SGD27 in Nordfjorden (Isfjorden). These surface signals defined the secondary MFA dimensions (Dimensions 3 and 2, respectively), confirming that surface-water variability is organized independently of the subsurface pattern.

Mosaic structure of biogeochemistry in western Svalbard fjords

Our data showed that deep water and porewater enrichment varied markedly among the inner sub-fjords of the Isfjorden system. Billefjorden and Dicksonfjorden are shallow-silled inner basins with less influence from Atlantic Water than the outer Isfjorden. Yet, they exhibit markedly different enrichment patterns, indicating that local basin morphology and circulation exert a

stronger influence on deep water and porewater biogeochemistry than the broader fjord-scale setting.

The fine-scale heterogeneity aligns with previous observations that Arctic fjords exhibit strong spatial variability driven by local hydrographic and geomorphological factors (Cottier *et al.* 2005; McGovern *et al.* 2020). Western Svalbard fjords display a mosaic spatial structure, a patchwork in which adjacent basins within the same fjord system have distinct biogeochemical conditions rather than a smooth fjord-wide gradient. This pattern is consistent with the established understanding of systems such as Isfjorden, where secondary fjords differ markedly in temperature, circulation, and biogeochemistry depending on sill depth, access to Atlantic Water, and proximity to land- and marine-terminating glaciers (Skogseth *et al.* 2020). In the same western Spitsbergen fjords, the distribution of inorganic carbon and the carbonate system is governed by the relative contributions of Atlantic Water, colder coastal-current water, and glacial freshwater (Fransson *et al.* 2015, 2016), consistent with the water-mass and freshwater controls on deep water and porewater biogeochemistry inferred here. Deep water and porewater enrichment develop where physical isolation and biogeochemical production coincide, whereas nearby sites in the same fjord can carry different chemical signatures even at similar depths or comparable proximity to land-based inputs. The role of proximity to freshwater sources such as river mouths and glacier fronts remains unclear in this dataset, since distance alone does not capture differences in discharge or freshwater composition among sources. Overall, however, the results indicate that deep water and porewater enrichment is more strongly controlled by restricted deep-water renewal than by proximity to land.

Because sampling was distributed across two summers (2021 and 2022), with each site visited only once, spatial and inter-annual variation cannot be fully separated in this dataset, and the pattern reported here should be interpreted in light of the inter-annual variability documented for these fjords. In Kongsfjorden, Fransson *et al.* (2016) found that a shift in the balance between Atlantic Water and the colder, CO_2-rich coastal current between 2013 and 2014 lowered summer pH and aragonite saturation in the year with weaker Atlantic inflow, and that the biological imprint on the carbonate system varied more between years than the freshwater imprint. In Tempelfjorden, Fransson *et al.* (2015) showed that an anomalously mild winter with delayed sea-ice formation during 2012 produced the highest freshwater fractions and the lowest saturation states in their record. Sea ice contributes directly: brine rejected during ice formation generates

dense, DIC-enriched water that can sink into the deeper basins, while the coastal current carries CO_2-rich, sea-ice-influenced water of Storfjorden origin into the western fjords. These processes act mainly on the surface and bottom waters and on the external source waters, rather than on the porewater enrichment described above, which is set by in-situ remineralization; they nonetheless imply that absolute concentrations, though not necessarily the layer-to-layer covariation structure, would differ in a year with contrasting ice cover or Atlantic inflow.

Implications for fjords under changing Arctic conditions

Projected changes in winter water formation, Atlantic Water intrusion, and freshwater inputs may alter the persistence of isolated bottom waters and the associated enrichment patterns. Reduced winter renewal, already observed in parts of the Svalbard fjords (Cottier *et al.* 2005), may prolong isolation in silled basins, whereas increased Atlantic inflow could enhance ventilation and disrupt locally accumulated deep water and porewater signals (Tverberg *et al.* 2019). Concurrent changes in primary production and terrestrial inputs due to glacial retreat and permafrost thaw (McGovern *et al.* 2020; Diak *et al.* 2023) may further influence whether fjord basins with restricted water renewal develop coordinated deep water and porewater enrichment.

The pronounced site-scale heterogeneity documented in this study suggests that responses to climate forcing will vary locally, complicating fjord-scale predictions of future nutrient and carbon dynamics (Fransson *et al.* 2015, 2016; Ericson *et al.* 2019a). The spatial organization revealed here indicates that predictive models of Arctic fjord biogeochemistry need to account for basin-scale heterogeneity and variations among secondary fjords and inner basins within larger systems, rather than relying solely on fjord-wide averages.

Conclusion

MFA of dissolved carbon and nutrient concentrations across five water column and sediment layers in western Svalbard fjords revealed strong covariation among bottom water, water above sediment, and porewaters, decoupled from the overlying surface water, which is set apart by summer stratification. Bottom water chemistry closely tracked porewater chemistry at the site scale, indicating that near-bottom waters integrate the sedimentary biogeochemical signal. Most deep water and porewater variability was driven by a few sites in restricted, poorly ventilated basins, where enrichment in DIC, DOC, NH_4^+, PO_4^{3-}, and DSi, as confirmed by concentration profiles and their relationships with Cl^-, reflected in situ remineralization rather than physical

mixing, producing local biogeochemical hotspots. Differences among sites within fjords were as great as, or even greater than, differences between fjord systems, pointing to a mosaic structure governed by local basin morphology and circulation rather than fjord-wide gradients. As winter water formation, Atlantic Water intrusion, and freshwater inputs shift under continued Arctic warming, this fine-scale heterogeneity implies that fjord-averaged predictions will miss biogeochemically important basins, and that resolving individual basins and secondary fjords will be essential for anticipating future carbon and nutrient dynamics.

Acknowledgements

We thank our colleagues (Beata Szymczycha, Przemysław Makuch, Magdalena Diak, Katarzyna Koziorowska, Aleksandra Winogradow, Laura Bromboszcz, Piotr Prusiński, Karol Kuliński, Miłosz Grabowski, and Marek Zajączkowski) for their ideas and assistance with fieldwork and technical support. We want to thank the captain and crew of r/v *Oceania*. The research leading to these results has received funding from the Norwegian Financial Mechanism 2014–2021 project no. 2019/34/H/ST10/00645 and 2019/34/H/ST10/00504. Additionally, the study is supported by the Institute of Oceanology Polish Academy of Sciences, through its statutory activities: task II.9. Authors thank two anonymous reviewers whose comments helped to improve this manuscript.

References

Abdi H., Williams L.J. and Valentin D. 2013. Multiple factor analysis: principal component analysis for multitable and multiblock data sets. *WIREs Computational Statistics* 5: 149–179, doi: 10.1002/wics.1246.

Azetsu-Scott K. and Syvitski J.P.M. 1999. Influence of melting icebergs on distribution, characteristics and transport of marine particles in an East Greenland fjord. J*ournal of Geophysical Research: Oceans* 104: 5321–5328, doi: 10.1029/1998JC900083.

Cottier F., Tverberg V., Inall M., Svendsen H., Nilsen F. and Griffiths C. 2005. Water mass modification in an Arctic fjord through cross-shelf exchange: The seasonal hydrography of Kongsfjorden, Svalbard. *Journal of Geophysical Research: Oceans* 110: C12005, doi: 10.1029/2004JC002757.

Diak M., Böttcher M.E., Ehlert von Ahn C.M., Hong W.-L., Kędra M., Kotwicki L., Koziorowska-Makuch K., Kuliński K., Lepland A., Makuch P., Sen A., Winogradow A., Silberberger M.J. and Szymczycha B. 2023. Permafrost and groundwater interaction: current state and future perspective. *Frontiers in Earth Science* 11: 1254309, doi: 10.3389/feart.2023.1254309.

Ericson Y., Chierici M., Falck E., Fransson A., Jones E. and Kristiansen S. 2019a. Seasonal dynamics of the marine CO_2 system in Adventfjorden, a West Spitsbergen fjord. *Polar Research* 38: 3345, doi: 10.33265/polar.v38.3345.

Ericson Y., Falck E., Chierici M., Fransson A. and Kristiansen S. 2019b. Marine CO_2 system variability in a high arctic tidewater-glacier fjord system, Tempelfjorden, Svalbard. *Continental Shelf Research* 181: 1–13, doi: 10.1016/j.csr.2019.04.013.

Fransson A., Chierici M., Nomura D., Granskog M.A., Kristiansen S., Martma T. and Nehrke G. 2015. Effect of glacial drainage water on the CO_2 system and ocean acidification state in an Arctic tidewater-glacier fjord during two contrasting years. *Journal of Geophysical Research: Oceans* 120: 2413–2429, doi: 10.1002/2014JC010320.

Fransson A., Chierici M., Hop H., Findlay H.S., Kristiansen S. and Wold A. 2016. Late winter-to-summer change in ocean acidification state in Kongsfjorden, with implications for calcifying organisms. *Polar Biology* 39: 1841–1857, doi: 10.1007/s00300-016-1955-5.

Görlich K. 1986. Glacimarine sedimentation of muds in Hornsund Fjord, Spitsbergen. *Annales Societatis Geologorum Poloniae* 56: 433–477.

Grasshoff K., Kremling K. and Ehrhardt M. (eds.) 1999. *Methods of Seawater Analysis.* Wiley, doi: 10.1002/9783527613984.

Hop H., Pearson T., Hegseth E.N., Kovacs K.M., Wiencke C., Kwasniewski S., Eiane K., Mehlum F., Gulliksen B., Wlodarska-Kowalczuk M., Lydersen C., Weslawski J.M., Cochrane S., Gabrielsen G.W., Leakey R.J.G., Lønne O.J., Zajaczkowski M., Falk-Petersen S., Kendall M., Wängberg S.-Å., Bischof K., Voronkov A.Y., Kovaltchouk N.A., Wiktor J., Poltermann M., Prisco G., Papucci C. and Gerland S. 2002. The marine ecosystem of Kongsfjorden, Svalbard. *Polar Research* 21: 167–208, doi: 10.1111/j.1751-8369.2002.tb00073.x.

Huettel M., Berg P. and Kostka J.E. 2014. Benthic exchange and biogeochemical cycling in permeable sediments. *Annual Review of Marine Science* 6: 23–51, doi: 10.1146/annurev-marine-051413-012706.

Inall M.E. and Gillibrand P.A. 2010. The physics of mid-latitude fjords: a review. *Geological Society, London, Special Publications* 344: 17–33, doi: 10.1144/SP344.3.

Jakobsson M., Mayer L., Coakley B. *et al.* 2012. The International Bathymetric Chart of the Arctic Ocean (IBCAO) Version 3.0. *Geophysical Research Letters* 39: L12609, doi: 10.1029/2012GL052219.

Jakobsson M., Mohammad R., Karlsson M. *et al.* 2024. The International Bathymetric Chart of the Arctic Ocean Version 5.0. *Scientific Data* 11: 1420, doi: 10.1038/s41597-024-04278-w.

Kleber G.E., Hodson A.J., Magerl L., Mannerfelt E.S., Bradbury H.J., Zhu Y., Trimmer M. and Turchyn A. V. 2023. Groundwater springs formed during glacial retreat are a large source of methane in the high Arctic. *Nature Geoscience* 16: 597–604, doi: 10.1038/s41561-023-01210-6.

Kłostowska Ż., Szymczycha B., Lengier M., Zarzeczańska D. and Dzierzbicka-Głowacka L. 2020. Hydrogeochemistry and magnitude of SGD in the Bay of Puck, southern Baltic Sea. *Oceanologia* 62: 1–11, doi: 10.1016/j.oceano.2019.09.001.

Kostka J., Thamdrup B., Glud R. and Canfield D. 1999. Rates and pathways of carbon oxidation in permanently cold Arctic sediments. *Marine Ecology Progress Series* 180: 7–21, doi: 10.3354/meps180007.

McGovern M., Pavlov A.K., Deininger A., Granskog M.A., Leu E., Søreide J.E. and Poste A.E. 2020. Terrestrial inputs drive seasonality in organic matter and nutrient biogeochemistry in a high arctic fjord system (Isfjorden, Svalbard). *Frontiers in Marine Science* 7: 542563, doi: 10.3389/fmars.2020.542563.

Meyer H.K., Roberts E.M., Mienis F. and Rapp H.T. 2020. Drivers of megabenthic community structure in one of the world's deepest silled-fjords, Sognefjord (Western Norway). *Frontiers in Marine Science* 7: 393, doi: 10.3389/fmars.2020.00393.

Nilsen F., Skogseth R., Vaardal-Lunde J. and Inall M. 2016. A simple shelf circulation model: Intrusion of Atlantic Water on the West Spitsbergen shelf. *Journal of Physical Oceanography* 46: 1209–1230, doi: 10.1175/JPO-D-15-0058.1.

Pawłowska J., Zajączkowski M., Łącka M., Lejzerowicz F., Esling P. and Pawlowski J. 2016. Palaeoceanographic changes in Hornsund Fjord (Spitsbergen, Svalbard) over the last millennium: new insights from ancient DNA. *Climate of the Past* 12: 1459–1472, doi: 10.5194/cp-12-1459-2016.

Piwosz K., Walkusz W., Hapter R., Wieczorek P., Hop H. and Wiktor J. 2009. Comparison of productivity and phytoplankton in a warm (Kongsfjorden) and a cold (Hornsund) Spitsbergen fjord in mid-summer 2002. *Polar Biology* 32: 549–559, doi: 10.1007/s00300-008-0549-2.

Promińska A., Falck E. and Walczowski W. 2018. Interannual variability in hydrography and water mass distribution in Hornsund, an Arctic fjord in Svalbard. *Polar Research* 37: 1495546, doi: 10.1080/17518369.2018.1495546.

Roy S., Hovland M., Noormets R. and Olaussen S. 2015. Seepage in Isfjorden and its tributary fjords, West Spitsbergen. *Marine Geology* 363: 146–159, doi: 10.1016/j.margeo.2015.02.003.

Saghravani S.R. 2026. Geochemical characteristics of deep-water cold seeps influenced by offshore Arctic groundwater discharge. *Marine Chemistry* 277: 104657, doi: 10.1016/j.marchem.2026.104657.

Saghravani S.R., Böttcher M.E., Hong W.-L., Kuliński K., Lepland A., Sen A. and Szymczycha B. 2024. Distributions of in situ parameters, dissolved (in)organic carbon, and nutrients in the water column and pore waters of Arctic fjords (western Spitsbergen) during a melting season. *Earth System Science Data* 16: 3419–3431, doi: 10.5194/essd-16-3419-2024.

Santos I.R., Chen X., Lecher A.L., Sawyer A.H., Moosdorf N., Rodellas V., Tamborski J., Cho H.-M., Dimova N., Sugimoto R., Bonaglia S., Li H., Hajati M.-C. and Li L. 2021. Submarine groundwater discharge impacts on coastal nutrient biogeochemistry. *Nature Reviews Earth and Environment* 2: 307–323, doi: 10.1038/s43017-021-00152-0.

Sejr M.K., Stedmon C.A., Bendtsen J., Abermann J., Juul-Pedersen T., Mortensen J. and Rysgaard S. 2017. Evidence of local and regional freshening of Northeast Greenland coastal waters. *Scientific Reports* 7: 13183, doi: 10.1038/s41598-017-10610-9.

Skogseth R., Haugan P.M. and Jakobsson M. 2005. Watermass transformations in Storfjorden. *Continental Shelf Research* 25: 667–695, doi: 10.1016/j.csr.2004.10.005.

Skogseth R., Olivier L.L.A., Nilsen F., Falck E., Fraser N., Tverberg V., Ledang A.B., Vader A., Jonassen M.O., Søreide J., Cottier F., Berge J., Ivanov B.V. and Falk-Petersen S. 2020. Variability and decadal trends in the Isfjorden (Svalbard) ocean climate and circulation – An indicator for climate change in the European Arctic. *Progress in Oceanography* 187: 102394, doi: 10.1016/j.pocean.2020.102394.

Smith R.W., Bianchi T.S., Allison M., Savage C. and Galy V. 2015. High rates of organic carbon burial in fjord sediments globally. *Nature Geoscience* 8: 450–453, doi: 10.1038/ngeo2421.

Stigebrandt A. 2012. Hydrodynamics and circulation of fjords. *In*: Bengtsson L., Herschy R.W. and Fairbridge R.W. (eds.) *Encyclopedia of Lakes and Reservoirs*. Dordrecht: Springer Netherlands: 327–344, doi: 10.1007/978-1-4020-4410-6_247.

Svendsen H., Beszczyńska-Møller A., Hagen J.O., Lefauconnier B., Tverberg V., Gerland S., Ørbøk J.B., Bischof K., Papucci C., Zajączkowski M., Azzolini R., Bruland O., Wiencke C., Winther J.-G. and Dallmann W. 2002. The physical environment of Kongsfjorden-Krossfjorden, an Arctic fjord system in Svalbard. *Polar Research* 21: 133–166, doi: 10.1111/j.1751-8369.2002.tb00072.x.

Swerpel S. 1985. The Hornsund fiord: Water masses. *Polish Polar Research* 6: 475–496.

Syvitski J.P.M. 1989. On the deposition of sediment within glacier-influenced fjords: Oceanographic controls. *Marine Geology* 85: 301–329, doi: 10.1016/0025-3227(89)90158-8.

Szczuciński W., Zajączkowski M. and Scholten J. 2009. Sediment accumulation rates in subpolar fjords – Impact of post-Little Ice Age glaciers retreat, Billefjorden, Svalbard. *Estuarine, Coastal and Shelf Science* 85: 345–356, doi: 10.1016/j.ecss.2009.08.021.

Szymczycha B., Diak M., Hong W.-L., Böttcher M.E., Lepland A., Makuch P., ten Hietbrink S., Saghravani S.R., Sen A., Winogradow A. and Silberberger M.J. 2025. Submarine groundwater discharge and gas hydrate dissociation fuel organic matter formation in Arctic fjord sediments. *Marine Chemistry* 273: 104570, doi: 10.1016/j.marchem.2025.104570.

Taniguchi M., Dulai H., Burnett K.M., Santos I.R., Sugimoto R., Stieglitz T., Kim G., Moosdorf N. and Burnett W.C. 2019. Submarine groundwater discharge: Updates on its measurement techniques, geophysical drivers, magnitudes, and effects. *Frontiers in Environmental Science* 7: 141, doi: 10.3389/fenvs.2019.00141.

Tverberg V., Skogseth R., Cottier F., Sundfjord A., Walczowski W., Inall M.E., Falck E., Pavlova O. and Nilsen F. 2019. The Kongsfjorden transect: Seasonal and inter-annual variability in hydrography. *In:* Hop H. and Wiencke C. (eds.) *The Ecosystem of Kongsfjorden, Svalbard*. Springer International Publishing: 49–104, doi: 10.1007/978-3-319-46425-1_3.

Vihtakari M. 2020. PlotSvalbard: PlotSvalbard - Plot research data from Svalbard on maps, https://github.com/MikkoVihtakari/PlotSvalbard.

Table 1. Selected environmental characteristics of sampling sites in four Svalbard fjords

Site	Fjord[a]	Date	Water Depth	Core penetration depth	Bottom water Temp	Distance from Glacier	Distance from Land	SW Cl^-	LP Cl^-
			(m)	(cm)	(°C)	(km)	(km)	(mmol L^{-1})	(mmol L^{-1})
SGD1	HR	2022	124	142.5	-1.2	5.0	2.2	490.5	399.9
SGD2	HR	2021	83	55	1.1	13.0	2.5	456.1	456.0
SGD3	HR	2021	240	280	1.6	6.7	2.7	502.7	505.9
SGD4	HR	2021	181	268.5	1.4	5.3	3.5	468.3	320.5
SGD5	HR	2021	53	90	1.5	3.7	1.7	477.7	335.4
JMW25	ISF	2021	33	85	3.1	2.5	1.1	486.0	455.6
IT3	ISF	2021	39.4	41.5	1.8	1.9	1.0	470.2	502.5
JMW4	ISF	2021	72	180	1.5	15.2	0.9	500.9	364.3
Yol2	ISF	2021	71	21.5	1.5	11.8	4.8	469.5	549.1
SGD9	ISF	2021	146	234	-1.7	13.1	1.9	528.8	525.8
SGD11	ISF	2022	65	130	2.4	1.7	1.7	503.4	562.5
DCK	ISF	2022	17	100.5	5.0	7.0	2.5	414.0	555.1
SGD21	ISF	2022	100	129.7	0.8	2.2	2.2	482.8	512.2
SGD27	ISF	2022	35	146	3.0	28.8	1.7	425.8	488.6
SGD23	KG	2022	153	128	2.5	3.4	2.2	468.5	565.2
SGD32	KG	2022	374	71.5	1.3	5.2	12.0	492.3	530.6
V1	KG	2022	98.4	113.5	2.9	2.2	1.8	490.5	547.2
SGD25	KR	2022	146	74.5	2.9	6.0	1.5	457.3	539.8
KL1	KR	2022	287	129.5	1.9	11.1	1.2	446.2	508.3

[a] HR - Hornsund; ISF - Isfjord; KG - Kongsfjord; KR - Krossfjord. SW - surface water; LP - lower porewater.

Table 2. Summary of MFA results for the first five retained dimensions. Eigenvalues and percentages of explained variance are shown for each dimension. "Main Contributing Groups" identify layers with group loadings > 0.40, indicating strong association with the corresponding dimension. "Key Site Contributors" represent sampling sites with the largest percentage contributions to each dimension's variance.

Dimension	Eigenvalue	Variance (%)	Cumulative (%)	Main Contributing Groups (Loading > 0.40)	Key Site Contributors
1	2.92	29.9	29.9	Bottom water (0.70) Water above sediment (0.72) Upper porewater (0.65) Lower porewater (0.72)	SGD9 (40.8%) SGD4 (18.0%) SGD3 (14.6%)
2	1.41	14.4	44.3	Surface water (0.56) Upper porewater (0.40)	SGD27 (23.9%) SGD5 (11.0%)
3	1.29	13.2	57.4	Surface water (0.50)	SGD5 (39.2%) SGD25 (13.0%)
4	0.89	9.1	66.5	None > 0.40	DCK (34.0%)
5	0.69	7.0	73.5	None > 0.40	SGD11 (21.4%)

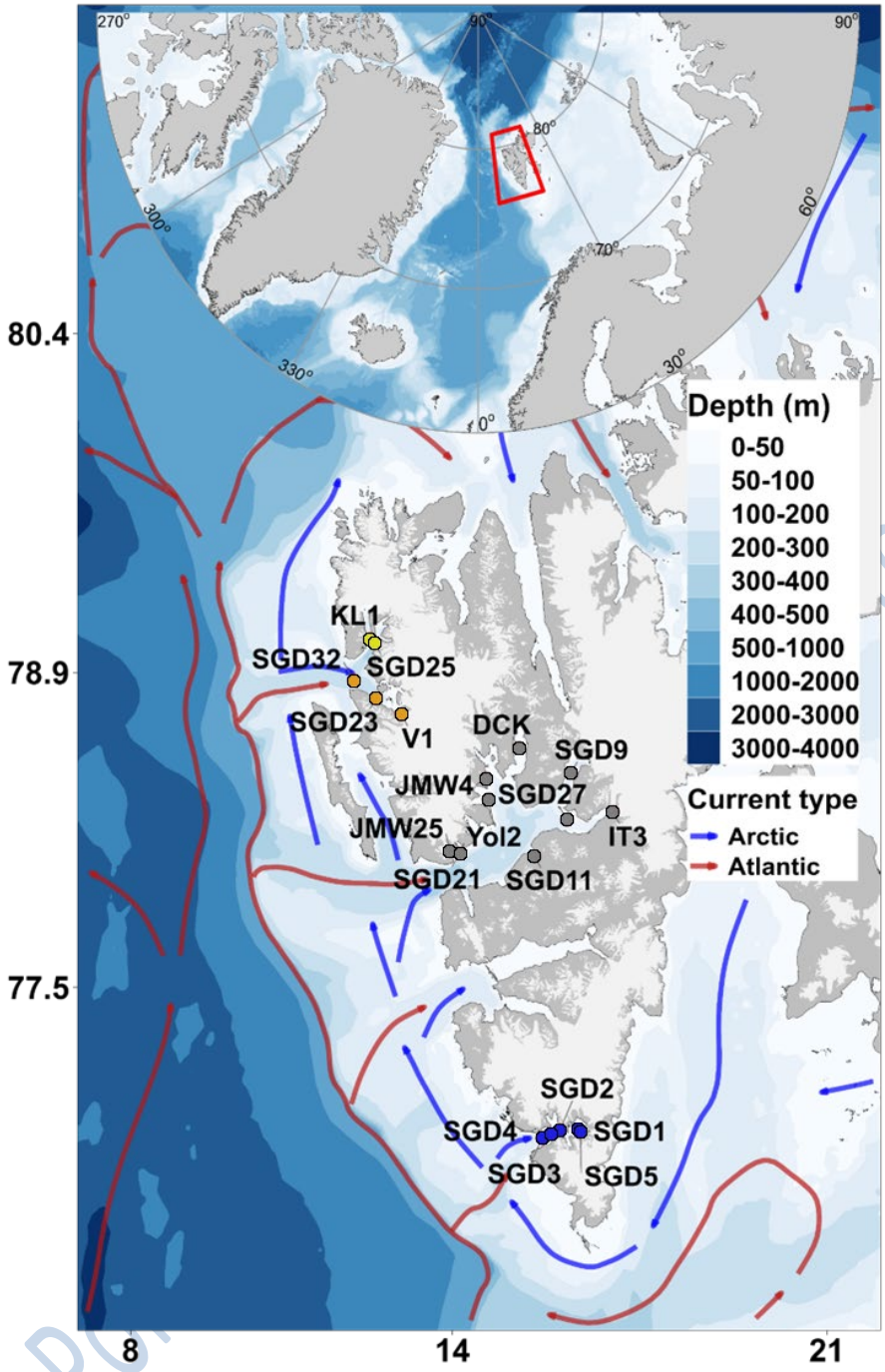

Fig. 1. Bathymetry of western Svalbard showing Atlantic (red) and Arctic (blue) current pathways and sampling sites in Krossfjord (yellow), Kongsfjorden (orange), Isfjorden (grey), and Hornsund (blue). Basemap data from GEBCO (Jakobsson *et al.* 2024), IBACO (Jakobsson *et al.* 2012), and PlotSvalbard (Vihtakari 2020).

Polish Polar Research
DOI: 10.24425/ppr.2026.3128

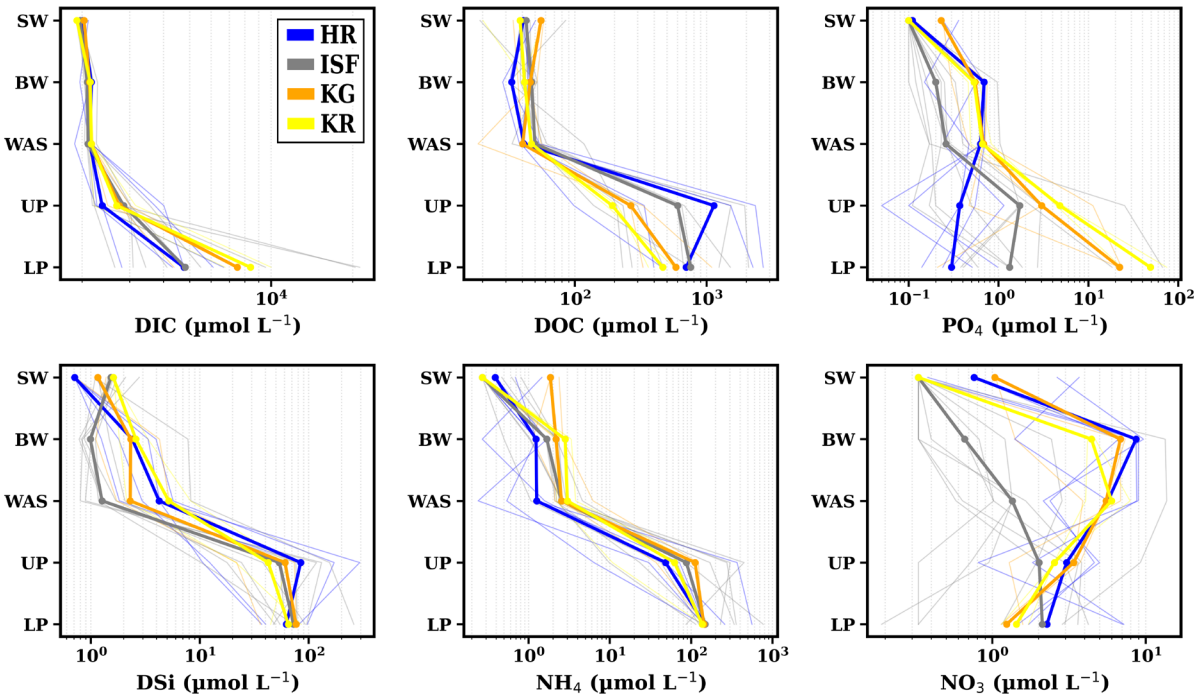

Fig. 2. Vertical concentration profiles of dissolved inorganic carbon (DIC), dissolved organic carbon (DOC), PO_4^{3-}, DSi, NH_4^+ and NO_3^- in the five sampled layers from surface downward: SW - surface water, BW - bottom water, WAS - water above sediment, UP - upper porewater, and LP - lower porewater. Thin lines are individual stations and bold lines are the median profile for each fjord; colors denote the fjords: HR - Hornsund (blue), ISF - Isfjorden (grey), KG - Kongsfjorden (orange), and KR - Krossfjorden (yellow).

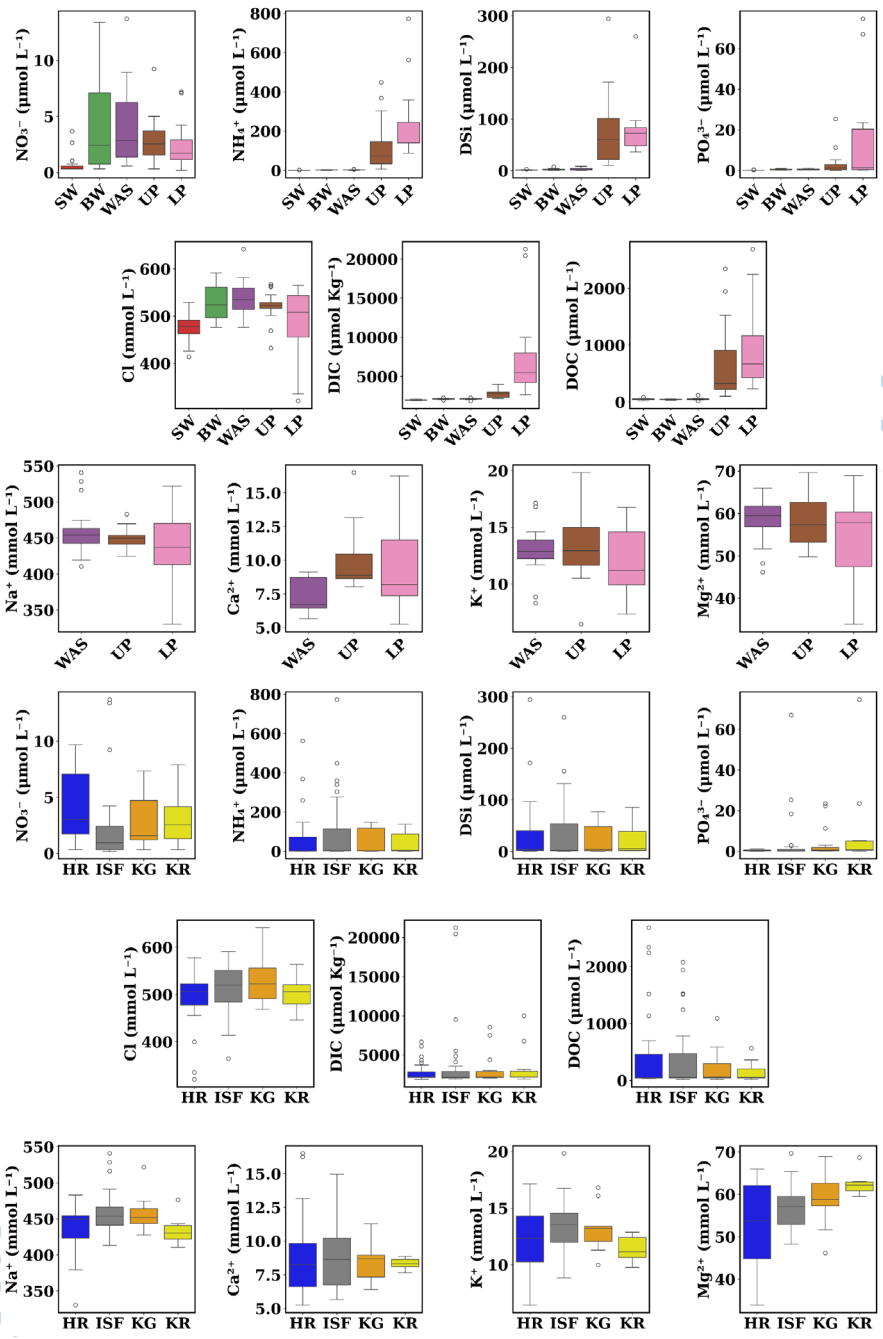

Fig. 3. Distributions of dissolved nutrients and carbon in water types and fjords. Box plots show NO_3^-, NH_4^+, DSi, PO_4^{3-}, Cl^-, DIC, DOC, and the major cations including Na^+, Ca^{2+}, K^+, and Mg^{2+}. The upper three rows group samples by water type, SW (surface water), BW (bottom water), WAS (water above sediment), UP (upper porewater) and LP (lower porewater), and the lower three rows group the same data by fjord: HR (Hornsund), ISF (Isfjorden), KG (Kongsfjorden) and KR (Krossfjorden). Cations are shown only for the WAS, UP and LP layers. Boxes span the interquartile range (IQR) with the median marked, whiskers extend to 1.5 × IQR, and points beyond the whiskers are plotted as outliers.

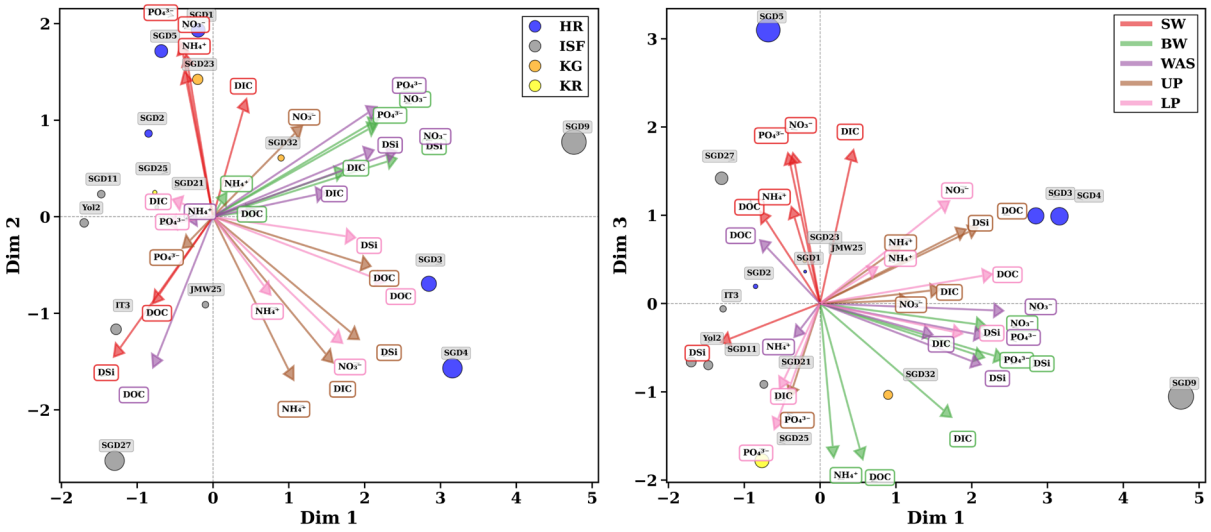

Fig. 4. Multiple factor analysis biplots in left panel: Dimension 1 (Dim 1) versus Dimension 2 (Dim 2); in right panel: Dimension 1 versus Dimension 3 (Dim 3) illustrating relationships among sampling sites and chemical variables in the first three ordination dimensions. Sampling sites are shown as colored points according to fjord system, with point size proportional to their cumulative contribution to the displayed dimensions. Larger points indicate sites with higher contributions to the variance of the corresponding dimensions. Site labels are shown in gray boxes. Variables are represented as arrows originating from the origin, with arrow direction indicating the gradient of increasing values and arrow length reflecting the strength of association with the ordination axes. Variables are color-coded by layer: SW - surface water (blue), BW - bottom water (green), WAS - water above sediment (purple), UP - upper porewater (brown), and LP - lower porewater (pink).

Polish Polar Research
DOI: 10.24425/ppr.2026.3128

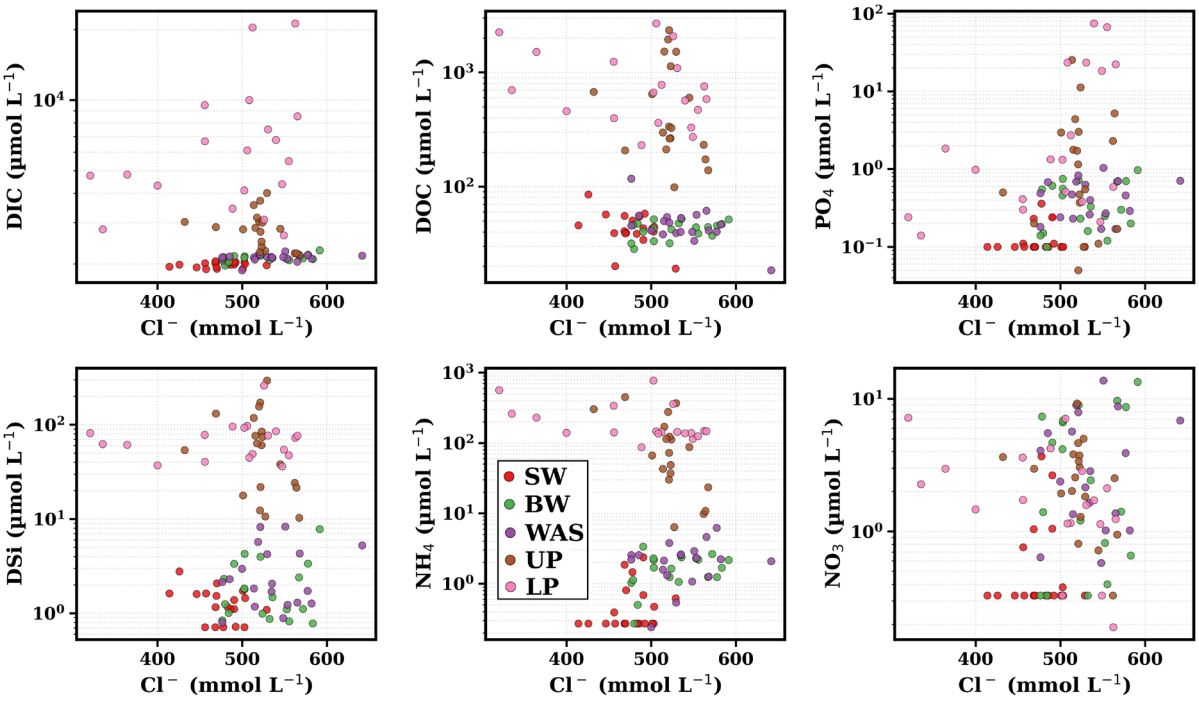

Fig. 5. Variables–chloride mixing diagrams for DIC, DOC, PO_4^{3-}, DSi, NH_4^+, and NO_3^-. Each point is a sample plotted against its Cl^-, used here as a conservative tracer of seawater–freshwater mixing; colors denote the water type including SW - surface water (blue), BW - bottom water (green), WAS - water above sediment (purple), UP - upper porewater (brown), and LP - lower porewater (pink).